Monoallelic and Biallelic Mutations in *MAB21L2* Cause a Spectrum of Major Eye Malformations

Joe Rainger,[1,16] Davut Pehlivan,[2,16] Stefan Johansson,[4,15,16] Hemant Bengani,[1,16] Luis Sanchez-Pulido,[6] Kathleen A. Williamson,[1] Mehmet Ture,[14] Heather Barker,[12] Karen Rosendahl,[7] Jürgen Spranger,[8] Denise Horn,[9] Alison Meynert,[1] James A.B. Floyd,[5] Trine Prescott,[10] Carl A. Anderson,[5] Jacqueline K. Rainger,[1] Ender Karaca,[2] Claudia Gonzaga-Jauregui,[2] Shalini Jhangiani,[3] Donna M. Muzny,[3] Anne Seawright,[1] Dinesh C. Soares,[13] Mira Kharbanda,[11] Victoria Murday,[11] Andrew Finch,[12] UK10K, Baylor-Hopkins Center for Mendelian Genomics, Richard A. Gibbs,[2,3] Veronica van Heyningen,[1] Martin S. Taylor,[1] Tahsin Yakut,[14] Per M. Knappskog,[4,15] Matthew E. Hurles,[5] Chris P. Ponting,[6] James R. Lupski,[2,3,17] Gunnar Houge,[4,17] and David R. FitzPatrick[1,17,*]

We identified four different missense mutations in the single-exon gene *MAB21L2* in eight individuals with bilateral eye malformations from five unrelated families via three independent exome sequencing projects. Three mutational events altered the same amino acid (Arg51), and two were identical de novo mutations (c.151C>T [p.Arg51Cys]) in unrelated children with bilateral anophthalmia, intellectual disability, and rhizomelic skeletal dysplasia. c.152G>A (p.Arg51His) segregated with autosomal-dominant bilateral colobomatous microphthalmia in a large multiplex family. The fourth heterozygous mutation (c.145G>A [p.Glu49Lys]) affected an amino acid within two residues of Arg51 in an adult male with bilateral colobomata. In a fifth family, a homozygous mutation (c.740G>A [p.Arg247Gln]) altering a different region of the protein was identified in two male siblings with bilateral retinal colobomata. In mouse embryos, *Mab21l2* showed strong expression in the developing eye, pharyngeal arches, and limb bud. As predicted by structural homology, wild-type MAB21L2 bound single-stranded RNA, whereas this activity was lost in all altered forms of the protein. MAB21L2 had no detectable nucleotidyltransferase activity in vitro, and its function remains unknown. Induced expression of wild-type *MAB21L2* in human embryonic kidney 293 cells increased phospho-ERK (pERK1/2) signaling. Compared to the wild-type and p.Arg247Gln proteins, the proteins with the Glu49 and Arg51 variants had increased stability. Abnormal persistence of pERK1/2 signaling in *MAB21L2*-expressing cells during development is a plausible pathogenic mechanism for the heterozygous mutations. The phenotype associated with the homozygous mutation might be a consequence of complete loss of MAB21L2 RNA binding, although the cellular function of this interaction remains unknown.

Structural eye malformations are an important cause of congenital visual impairment.[1,2] The terms anophthalmia and microphthalmia are used to indicate the absence or marked reduction in size, respectively, of an eye. Ocular coloboma (MIM 216820) describes the spectrum of eye malformations, including microphthalmia, resulting from failure of optic fissure closure during embryogenesis. These malformations show marked phenotypic and etiological heterogeneity. The most common identifiable genetic causes of structural eye malformations are those involving dosage-sensitive transcription factors (encoded by *SOX2* [MIM 184429],[3,4] *OTX2* [MIM 600037],[5] and *PAX6* [MIM 607108][6]) and retinoic acid metabolism or transport (regulated by *STRA6* [MIM 610745],[7] *ALDH1A3* [MIM 600463],[8] *RARB* [MIM 180220][9]). The cause in a significant proportion of individuals with major eye malformations, particularly in those with microphthalmia and coloboma,[10,11] remains unknown.

To further elucidate the genetic architecture of ocular coloboma, we performed exome sequencing on genomic DNA from an affected uncle and nephew (individuals II.6 and III.1) in a large family (family 1463) in which apparently isolated bilateral coloboma segregates in a pattern consistent with autosomal-dominant inheritance (Figure 1; Figure S3 and Table S2, available online). These were two of the 99 exome sequences (75 individuals with coloboma and 24 unaffected relatives from 58 different families) that comprised the coloboma contribution to the rare-diseases component of the UK10K project.[12] This study was approved by the UK Multiregional Ethics Committee

[1]Medical Research Council Human Genetics Unit, Medical Research Council Institute of Genetics and Molecular Medicine, Edinburgh EH4 2XU, UK; [2]Department of Molecular and Human Genetics, Baylor College of Medicine, One Baylor Plaza, 604B, Houston, TX 77030, USA; [3]Human Genome Sequencing Center, Baylor College of Medicine, One Baylor Plaza, MS BCM225, Houston, TX 77030, USA; [4]Center for Medical Genetics and Molecular Medicine, Haukeland University Hospital, Jonas Liesvei 65, 5021 Bergen, Norway; [5]Wellcome Trust Sanger Institute, Genome Campus, Hinxton, Cambridge CB10 1SA, UK; [6]Medical Research Council Functional Genomics Unit, Department of Physiology, Anatomy, and Genetics, University of Oxford, South Parks Road, Oxford OX1 3PT, UK; [7]Paediatric Radiology Department, Haukeland University Hospital, 5021 Bergen, Norway; [8]Im Fuchsberg 14, D76547 Sinzheim, Germany; [9]Institut für Medizinische Genetik, Charité Campus Virchow-Klinikum, 13353 Berlin, Germany; [10]Medical Genetics, Oslo University Hospital, 0424 Oslo, Norway; [11]Clinical Genetics, Southern General Hospital, Glasgow G51 4TF, UK; [12]Edinburgh Cancer Research Centre, Medical Research Council Institute of Genetics and Molecular Medicine, Edinburgh EH4 2XU, UK; [13]Centre for Genomics and Experimental Medicine, Medical Research Council Institute Genetics and Molecular Medicine, Edinburgh EH4 2XU, UK; [14]Department of Medical Genetics, University of Uludag, 16120 Bursa, Turkey; [15]Department of Clinical Science, University of Bergen, 5020 Bergen, Norway
[16]These authors contributed equally to this work
[17]These authors contributed equally to this work
*Correspondence: david.fitzpatrick@igmm.ed.ac.uk
http://dx.doi.org/10.1016/j.ajhg.2014.05.005.

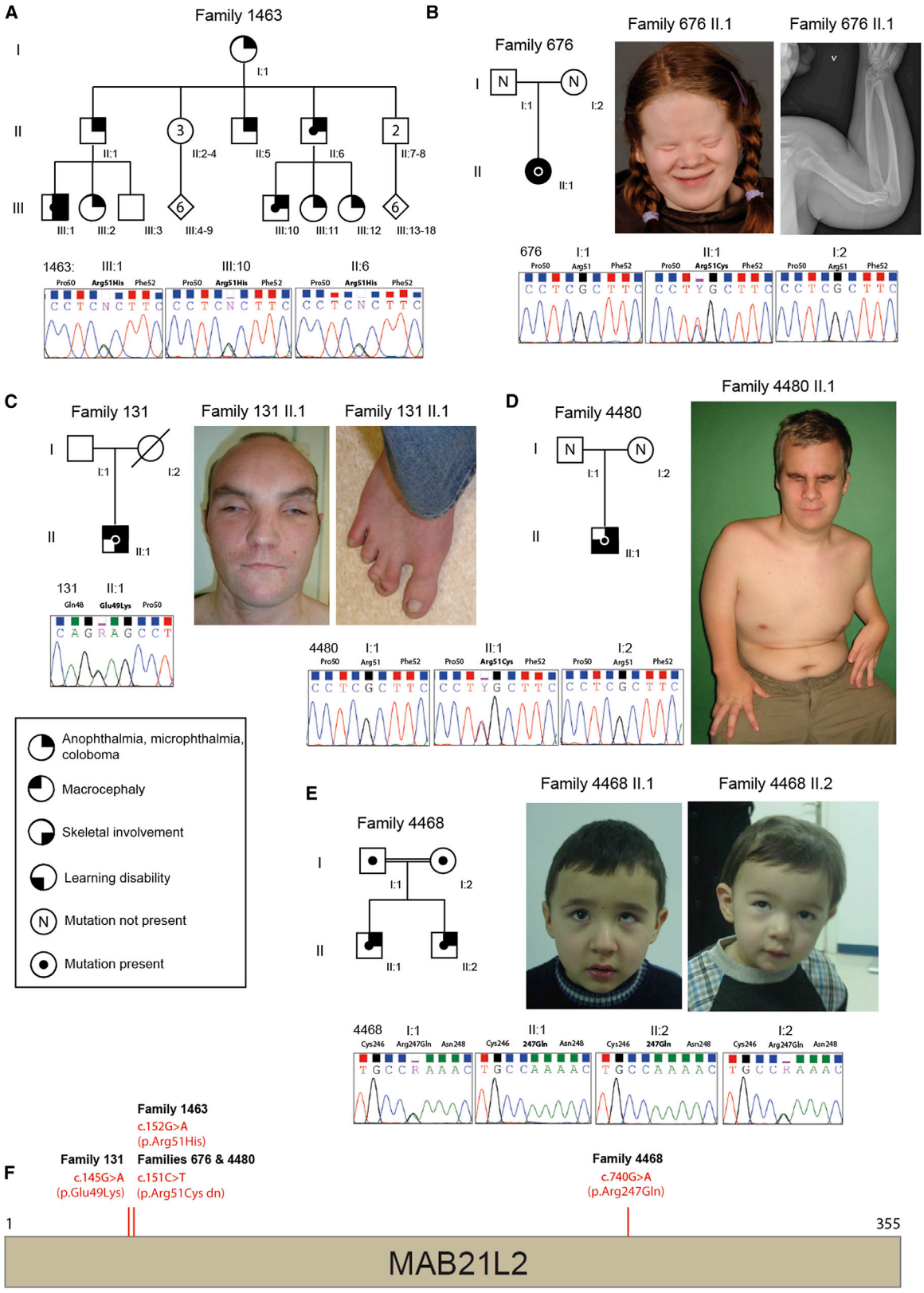

Figure 1. Family Structures and *MAB21L2* Mutations

(A–E) Diagrammatic representation of the structure of the five families—1463 (A), 676 (B), 131 (C), 4480 (D), and 4468 (E)—in whom mutations were identified in *MAB21L2*. The family number is given above each pedigree, and the sequencing chromatograms of the mutated base are given below each pedigree. Clinical images associated with each of the probands are located on the right-hand side of each cognate pedigree.

(F) The location of each missense mutation is provided on a schematic representation of MAB21L2.

(reference 06/MRE00/76), and informed consent was obtained from all participating families. Exome sequencing was performed as previously described.[13] Sequences were aligned with the Burrows-Wheeler Aligner v.0.5.9, duplicates were marked with Picard v.1.43, realignment around indels and base quality scores were recalibrated with the Genome Analysis Toolkit (GATK) v.1.0.5506, and variants were called only with GATK Unified Genotyper. The coverage and depth metrics for these exomes and for each of the other exome analyses mentioned below are provided in Table S4. A total of 27 shared heterozygous, rare (maximum allele frequency < 0.005 and mutation count in UK10K coloboma exomes < 3) variants were identified (Table S1). Two frameshift and one in-frame deletion were called in *IFT122* (MIM 606045) but were the result of misalignment of a single *IFT122* heterozygous frameshift mutation causing autosomal-recessive cranioectodermal dysplasia (MIM 218330). All the remaining missense mutations or in-frame deletions affected different genes. Only one mutation (c.152G>A [p.Arg51His]; chr4: g.151504333G>A) was found to alter a gene (*MAB21L2* [MIM 604357]) on our previously compiled list of 38 candidate genes for eye malformations (Table S3). This mutation is not reported in public databases, including the 1000 Genomes Project, the NHLBI Exome Sequencing Project (ESP) Exome Variant Server, and the Medical Research Council Human Genetics Unit in-house database of variants derived from ~2,200 exomes. The RefSeq accession numbers NM_006439.4 and NP_006430.1 were used for naming this and all subsequent *MAB21L2* variants at cDNA and protein levels, respectively. The entire UK10K coloboma exome data set is available from the European Genome-phenome Archive under a data-access agreement as study number EGAS00001000127.

Independently, trio whole-exome sequencing of an affected Norwegian female (II.1 in family 676 [Figure 1]) with bilateral anophthalmia, macrocephaly, moderate intellectual disability, and generalized skeletal dysplasia (Table S2) and her parents was performed as previously described[14] as part of a study approved by the Regional Committee for Medical and Health Research Ethics in western Norway (institutional review board [IRB] 00001872; written informed consent was obtained from the family). A total of 217 rare variants (with a maximum allele frequency < 0.005 in 1000 Genomes and not present in 80 in-house-generated Norwegian exome samples from the same pipeline) were detected in the proband and filtered against parental exome data in a search for putative de novo variants. Using this approach, we detected four variants, of which only one (c.151C>T [p.Arg51Cys]; chr4: g.151504332C>T; in *MAB21L2*) was confirmed by Sanger sequencing. This de novo missense mutation was found to alter the same amino acid (Arg51) as that in family 1463. The substitution changes a strictly conserved residue, and both p.Arg51Cys and p.Arg51His are predicted to be deleterious by SIFT, PolyPhen2, and AlignGVGD. Subsequently, one of the authors identified an unrelated male individual (II.1 in family 4480) with more severe rhizomelic skeletal dysplasia associated with bilateral anophthalmia (Figure 1; Table S2). Analysis of DNA samples from this individual and his parents was performed as part of the study approved by the UK Multiregional Ethics Committee (reference 06/MRE00/76; informed consent was obtained from the family). Exactly the same mutation (c.151C>T [p.Arg51Cys]), which had also occurred de novo, was identified in the affected child. Microsatellite analysis of the DNA samples from each family was performed to confirm biological relationships and to exclude sample mix up. The de novo mutation c.151C>T (p.Arg51Cys) thus has a clinically recognizable phenotype.

Resequencing of *MAB21L2* was performed in 336 unrelated individuals with major eye malformations (and with no overlap with those who were exome sequenced) as part of the study approved by the UK Multiregional Ethics Committee (reference 06/MRE00/76; informed consent was obtained from all participating families). This analysis revealed one different ultra-rare (not present in the NHLBI ESP Exome Variant Server, 1000 Genomes, or UK10K variant databases) heterozygous missense mutation (Figure 1) in the simplex case of an adult male with bilateral colobomatous microphthalmia (individual II.1 in family 131 [Figure 1; Table S2]). This mutation (c.145G>A [p.Glu49Lys]; chr4: g.151504326G>A) affects the codon encoding a residue two amino acids N-terminal to the substitutions identified above (p.Arg51His and p.Arg51Cys). This man had a history of reasonably good vision until the age of 11 years, after which he became blind over a period of 2 years. He had no evidence of retinal detachment at the age of 30 years, and no retinal electrophysiology was available. He was of normal intelligence and had only minor skeletal dysmorphisms, recurrent dislocation of the patellae, and soft-tissue syndactyly of the third and fourth digits of his hands and of the second and third digits of both feet (Table S2). His mother was deceased, and therefore we were unable to confirm whether this mutation had occurred de novo in this man.

A third independent exome sequencing study of distinct clinical phenotypes in children of consanguineous parents was carried out at the Baylor-Johns Hopkins Center for Mendelian Genomics under ethical approval from the Baylor College of Medicine (BCM) IRB (informed consent was obtained from all participating families). Two male siblings born to first-degree cousins were referred for clinical genetic assessment as a result of eye abnormalities. With the exception of subtle facial dysmorphic features and the eye findings, both boys had normal development. The elder boy (II.1 in family 4468) had left-eye esotropia in addition to a prominent forehead, periorbital fullness, long eyelashes, epicanthus, and a long and prominent philtrum (Table S2). Ophthalmologic examination revealed retinal coloboma including the optic disc and macula in the right eye, whereas there was sparing of the optic disc and macula in the left eye. Refractions were +2.0/+3.0 × 170

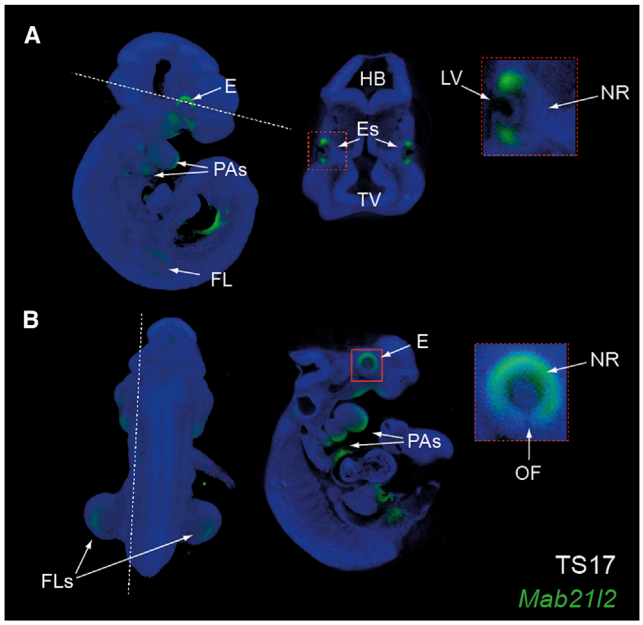

Figure 2. *Mab21l2* Expression during Mouse Eye Development
OPT images of *Mab21l2* expression at mouse Theiller stage 17 (TS17; 10.5 dpc). Hatched lines indicate the digital sections presented.
(A) Lateral 3D OPT projection showing *Mab21l2* expression in the eye (E), pharyngeal arches (PAs), and forelimbs (FLs). The transverse digital section presented alongside shows specific expression in the eyes, and an enlarged image (box) illustrates *Mab21l2* expression at the distal regions of the neural retina (NR), but not in the lens vesicle (LV).
(B) Posterior 3D OPT view illustrating specific *Mab21l2* expression in the FLs. The sagittal digital section presented alongside and the enlarged box illustrate that *Mab21l2* expression was highest dorsally but continued ventrally into the margins of the optic fissure (OF).
Further abbreviations are as follows: HB, hindbrain; and TV, telencephalic vesicle.

and −5.25/−3.25 × 115 in the right and left eyes, respectively. His younger brother (II.2 in family 4468) had right-eye exotropia and microphthalmia in addition to similar facial dysmorphic features. Ophthalmologic examination revealed bilateral retinal coloboma involving the optic disc in the right, but not the left, eye. Refractions were −2.00/−2.00 × 90 and +0.25/−1.50 × 175 in the right and left eyes, respectively. The parents of these siblings had normal vision and had no evidence of an asymptomatic structural eye malformation on ophthalmological examination.

Whole-exome sequencing in both affected siblings identified a homozygous nonsynonymous substitution (c.740G>A [p.Arg247Gln]; chr4: g.151504921G>A, hg19; RefSeq NM_006439) in *MAB21L2* in both brothers. This mutation has not been reported in public databases, including the 1000 Genomes Project, the NHLBI ESP Exome Variant Server, and the Atherosclerosis Risk in Communities Study database. In addition, this p.Arg247Gln substitution was not identified in an in-house-generated exome variant database from ~2,500 individuals at the BCM Human Genome Sequencing Center and BCM Whole Genome Laboratory Database, which includes anonymized data from over 1,000 individuals tested for diagnostic purposes. Sanger sequencing was performed for segregation analysis, and the parents were found to be heterozygous carriers, consistent with Mendelian expectation. All experiments and analyses were performed according to previously described methods.[15]

The human gene is named after the ortholog in *C. elegans*. Mutations in *Mab-21* cause posterior-to-anterior homeotic transformation of sensory ray 6 in the male tail in this worm.[16] In normal development, Mab-21 has been shown to interact with Sin-3, a key component of a histone-deacetylase-containing transcriptional regulatory complex,[17] and to be negatively regulated by CET-1 (whose human paralogs are BMP2, BMP4, and BMP7) signaling. After the identification of Mab-21 in *C. elegans*, multiple orthologous proteins were identified in human[18] and mouse.[19] In zebrafish, expression of *mab21l2* in the eye field is *rx3* dependent. Morpholino knockdown of *mab21l2* has been shown to produce a proliferation defect within the retinal progenitor cell population, resulting in small but structurally normal eyes.[20] Analysis of the *cis*-regulatory elements surrounding mab21l2 has identified functionally significant subpopulations of cells within the developing eye,[21] although the role of the gene product in the formation or maintenance of these cells is not yet clear. Homozygous targeted inactivation of *Mab21l2* in mouse embryos causes defects of the ventral body wall, severe eye malformations, and death in midgestation, whereas heterozygous null animals are apparently normal.[22] Homozygous null embryos show failure of lens induction and aplasia of the retinal pigment epithelium as a result of a proliferation defect within the optic vesicle. Given the severity of the phenotype observed in the *Mab21l2*-null mouse embryos and the relatively mild phenotype in the siblings homozygous for c.740G>A (p.Arg247Gln), it seems likely that the human mutation does not result in complete loss of function.

Although developmental expression of *Mab21l2* in mouse embryos has been previously reported,[23] we wished to examine the expression in the developing eye in more detail. A digoxigenin-labeled antisense riboprobe targeted to the 5′ UTR of *Mab21l2* (chr3: 86,547,729–86,548,237, mm10) was used for whole-mount in situ hybridization of 9.5, 10.5, 11.5, and 12.5 day postcoitum (dpc) mouse embryos (Figure S3). In addition to bright-field imaging, optical projection tomography (OPT) was also used for visualizing 10.5 dpc embryos as previously described.[12] We chose 10.5 dpc for full descriptive analysis because this time point is prior to optic fissure closure but has a well-formed optic cup. Strong expression was evident in the rostral and distal regions of the developing neural retina (Figure 2A), and there was no expression immediately adjacent to the closing optic fissure (Figure 2B). Expression was also observed in the dorsal and ventral aspects of the developing forelimb bud and in the developing pharyngeal arches. The

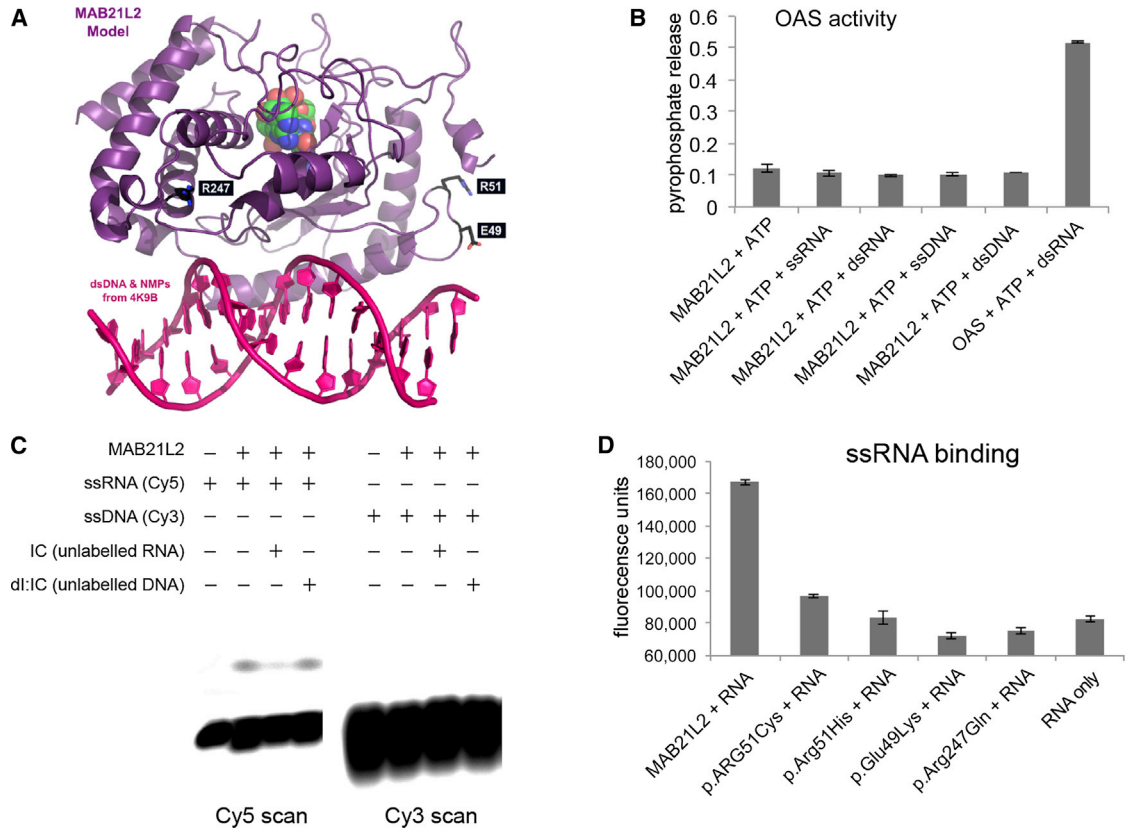

Figure 3. Structural Modeling of MAB21L2 and Prediction of Nucleotidyltransferase Activity

(A) A model of MAB21L2 was generated with PDB 4K9B as a template and is shown in purple; the nucleotide monophosphates are shown in green, blue, and red. This analysis suggests that MAB21L2 has both a nucleotidyltransferase active site and a DNA- and/or RNA-binding domain (double-stranded DNA is shown in pink in the foreground). The position of the residues that were altered in the affected individuals is shown in white text in black boxes. The arginine residues (Arg51 [R51] and Arg247 [R247]) are highlighted in blue, and the glutamic acid residue (Glu49 [E49]) is shown in orange.

(B) A graph showing the absence of OAS-like activity in purified MAB21L2. When OAS protein purified in the same way as MAB21L2 was incubated with ATP and double-stranded RNA (dsRNA), significant pyrophosphate release was detected, indicating nucleotidyltransferase activity. MAB21L2 showed no activity above background with ATP (or other nucleoside triphosphates [Figure S2]) using dsRNA, double-stranded DNA, ssRNA, or ssDNA as an activator.

(C) An electromobility shift assay (EMSA) using fluorescently labeled I:C oligonucleotides shows binding of wild-type MAB21L2 to ssRNA, but not ssDNA. The ssRNA binding could be completed efficiently with unlabeled ssRNA, but not ssDNA.

(D) Solution-based assay showing that wild-type MAB21L2 could efficiently bind a digoxigenin-labeled ssRNA molecule (this was an antisense riboprobe against *FZD5*, but all probes tested behaved in an identical fashion). None of the altered proteins could bind the ssRNA probe at levels above background.

The error bars in (B) and (D) represent SE. Each experiment represents readings from two biological replicates, and all experiments were repeated twice.

site- and stage-specific developmental expression pattern of *Mab21l2* is thus compatible with the eye and limb phenotypic effects associated with the mutations we identified above. No *Mab21l2* expression was observed in the brain at 10.5 dpc on OPT. However, imaging of more intensely stained embryos showed striking midbrain expression of *Mab21l2* at 9.5 and 10.5 dpc (Figure S3). This might be important in view of the neurodevelopmental problems reported in the individuals (676 II.1 and 4480 II.1) carrying the substitution p.Arg51Cys.

The highly localized distribution of the heterozygous missense mutations suggests a mutational mechanism that might not be simple loss of function. The biochemical function of MAB21L2 is not known, but the residues at which each of the amino acid substitutions occurred (Glu49, Arg51, and Arg247) in the human protein are completely conserved in mouse, zebrafish, and *C. elegans* (Figure S1). The family of 12 human Mab-21 paralogs adopt a nucleotidyltransferase fold[24] and include a cyclic GMP-AMP synthase (cGAS), which generates cyclic GMP-AMP in the cytoplasm of cells exposed to DNA.[25] Detailed examination of the structure of both cGAS (Protein Data Bank [PDB] accession number 4K9B) and another family member, RNA-activated antiviral protein 2′-5′-oligoadenylate synthetase (OAS[26] [PDB 1PX5]), indicated conservation of the active site in MAB21L2 (Figure 3A). However, a sensitive colorimetric assay using purified MAB21L2 (from *E. coli* or human embryonic kidney 293 [HEK293] cells) with ATP as a substrate (Figure 3B) for analysis of pyrophosphate release[27] detected no nucleotidyltransferase

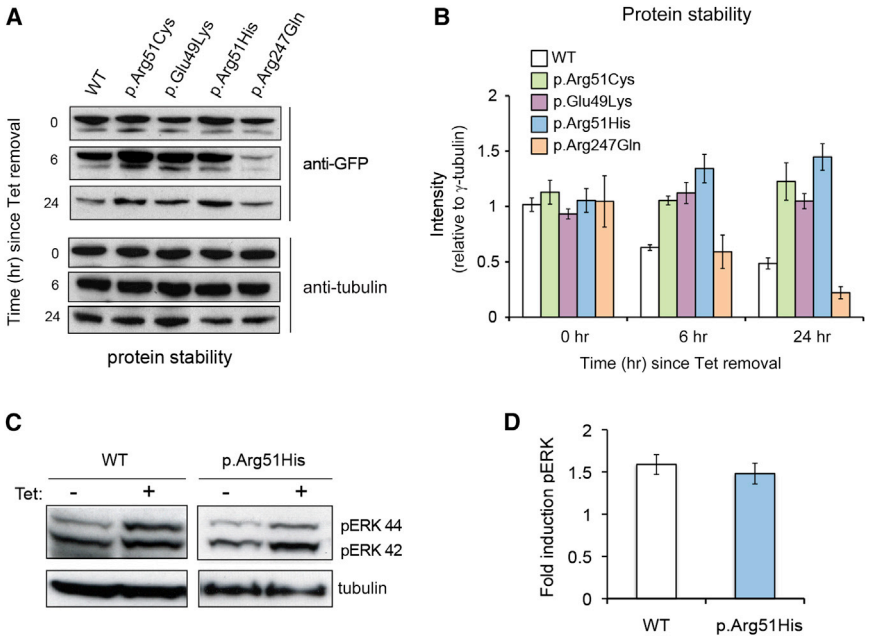

Figure 4. Protein Stability Estimations and Induction of ERK Signaling by MAB21L2

(A) Time-course analysis of protein stability with the use of anti-GFP immunoblotting of MAB21L2 at various time points since tetracycline (Tet) removal. Data presented are representative of five independent replicates.

(B) Quantification of immunoblots indicates higher protein stability for the proteins with substitutions at Glu49 or Arg51 than for the WT, whereas p.Arg247Gln displayed a pattern of protein stability similar to that of the WT. Error bars represent 95% confidence intervals.

(C) Increase in the level of the 44 kDa phospho-ERK band after 5 hr of Tet induction of WT and p.Arg51His MAB21L2 in inducible HEK293 cells.

(D) Graph representing quantification of this induction. Error bars represent 95% confidence intervals.

activity, whereas OAS purified by the same methods resulted in strong activity. This analysis was repeated with a mixture of all nucleoside triphosphates (Figure S2) with different plausible activator molecules (double-stranded RNA or DNA and single-stranded RNA [ssRNA] or DNA [ssDNA]), but no enzymatic activity was detectable for MAB21L2.

Enzymatic activation of OAS and cGAS occurs via conformational changes induced by binding with RNA and DNA, respectively.[28] The structural comparisons suggested that a ~35 Å long RNA- or DNA-binding groove also exists in MAB21L2 (Figure 3A; Figure S1). A fluorescent electromobility shift assay using Cy5- or Cy3-labeled ssRNA and ssDNA oligonucleotides and bacterially expressed protein showed binding of MAB21L2 to ssRNA, but not ssDNA (Figure 3C). To investigate the effect on ssRNA binding in each of the mutants (Figure 3D), we incubated a digoxigenin-labeled ssRNA (500 nt in length) in solution with sepharose-bead-bound wild-type or altered protein. After extensive washing, the binding of ssRNA to MAB21L2 was determined by fluorometry with an anti-digoxigenin-fluorescein antibody (Roche). Each of the four mutations, including the recessive mutation, resulted in loss of ssRNA-binding activity, consistent with the predicted locations of the affected residues close to the OAS RNA-binding cleft (Figure 3A). Complete loss of RNA binding in association with each of the mutations was remarkable but clearly cannot explain why the c.740G>A (p.Arg247Gln) variant is recessive and the other variants are dominant. We also had no knowledge of what the functional consequence of RNA binding was in the wild-type protein.

We therefore created multiple independent stable tetracycline-inducible HEK293 cell lines expressing the wild-type MAB21L2 and each of the altered forms as full-length GFP-fusion proteins. We used this system first to accurately determine the stability of the induced proteins by using a timed pulse of tetracycline. These analyses showed that all three of the monoallelic mutations resulted in significant stabilization of the protein in comparison to either the wild-type protein or the p.Arg247Gln variant (Figures 4A and 4B). Similar stabilization of altered protein has been reported in the recurrent de novo *PACS1* mutations, associated with characteristic facial dysmorphisms and significant intellectual disability.[29] In this study, they observed cytoplasmic aggregates of altered GFP-tagged protein, but we could identify no obvious aggregation or localization differences in the MAB21L2 variants (Figure S4). No predicted ubiquitination site could be located in the vicinity of the MAB21L2 substitutions. However, failure of the altered proteins to be recognized by the ubiquitin-mediated degradation system is the most likely mechanism for this observation.[30]

Given the above-mentioned data from *C. elegans*, we used the inducible cell system to identify any MAB21L2-dependent alteration in SMAD family member 1, 5, and 8 (SMAD1/5/8) signaling or extracellular-signal-regulated kinase 1 and 2 (ERK1/2) signaling. Immunoblots using anti-phospho-SMAD1/5/8 antibodies detected no alteration in canonical BMP signaling between cells expressing tagged *MAB21L2* and the same cells cultured without tetracycline (data not shown). However, induction of wild-type *MAB21L2* consistently resulted in an ~1.5-fold increase in 44 kDa phospho-ERK1 detected on immunoblot (Figures 4C and 4D). A similar level of induction was noted with the p.Arg51His substitution (Figures 4C and 4D). In mouse models of Noonan syndrome, an activating mutation in *Ptpn11* has been expressed as a transgene with the use of different tissue-specific promoters. Expression in the developing heart[31] and craniofacial region[32] produced

ERK upregulation associated with specific developmental defects. These malformations disappeared if the transgene was expressed in an ERK1/2-null background[31] or when ERK1/2 signaling was chemically ablated.[32] The pattern of malformations associated with ERK-activating mutations thus probably reflects the developmental expression of the mutated gene. ERK1/2-mediated signaling is active during eye and skeletal development and is almost entirely dependent on FGF receptor in the early mouse embryo.[33] The combination of protein stabilization and phospho-ERK (pERK1/2) induction suggests that the mutational mechanism in the monoallelic mutations affecting MAB21L2 might be activating mutations. Overactive pERK1/2 signaling is generally considered oncogenic, but a paradoxical growth inhibitory effect in chondrocytes has been recently proposed to explain how activating mutations in *FGFR3* (MIM 134934) can cause achondroplasia (MIM 100800) and thanatophoric dysplasia (MIM 187600).[34] In this model, pERK1/2 overactivity induces cellular defense mechanisms, which are potent inhibitors of growth. Such a mechanism could explain the rhizomelic skeletal dysplasia that is seen to be associated with *MAB21L2* mutations. However, given that the wild-type protein and the p.Arg51His substitution result in similar levels of ERK1/2 induction (1.5-fold; Figure 4), the important aspect might be the inability to control the precise timing of the pathway activity during critical developmental processes rather than the absolute level of signaling. The timing of ERK1/2 signaling is known to be crucial for the oscillatory expression of cyclic genes during somitogenesis,[35] but it is not yet clear which processes during ocular and skeletal development, if any, are timing critical. ERK1/2 signaling has not been examined in either mouse or zebrafish models for *Mab21l2* or *mab21l2* loss of function, respectively. However, "knocking in" these monoallelic mutations will be the most effective method of answering the precise relationship among these variants, ERK1/2 signaling, and the developmental pathology.

This report provides compelling human genomic and genetic evidence that mutations in *MAB21L2* cause major eye malformations. The combination of dominant and recessive mutations is intriguing, particularly given that the carriers of homozygous mutations are the least severely affected. The restricted repertoire of mutations in the monoallelic cases strongly suggests an unusual genetic mechanism. A similar restricted pattern is seen in disorders caused by the activation of signaling pathways, such as RASopathy disorders[36] and Myhre syndrome (MIM 139210).[37] It is possible that the monoallelic mutations act as dominant negative. The association between the monoallelic mutations and increased protein stability and the association between MAB21L2 and the induction of pERK signaling raise the possibility that aberrant persistence of a developmental signal might be the mechanism operating in those cases. It could be that complete loss of MAB21L2 RNA-binding activity in association with the recessive Arg247Gln variant might be producing the eye phenotype via a different mechanism, and as such, identifying the in vivo role of the RNA-binding activity is a priority for future work. An understanding of the cellular and developmental function of wild-type MAB21L2 will enable adequate interpretation of mutations at this locus in a clinical setting. Finally, this study illustrates the cumulative value of the active sharing of DNA variation observed in individual patients in order to aggregate sufficient evidence to support specific biological hypotheses.

Supplemental Data

Supplemental Data include four figures and four tables and can be found with this article online at http://dx.doi.org/10.1016/j.ajhg.2014.05.005.

Consortia

The members of the UK10K Rare Diseases Working Group are Matthew Hurles, David R. FitzPatrick, Saeed Al-Turki, Carl Anderson, Inês Barroso, Philip Beales, Jamie Bentham, Shoumo Bhattacharya, Keren Carss, Krishna Chatterjee, Sebhattin Cirak, Catherine Cosgrove, Allan Daly, Jamie Floyd, Chris Franklin, Marta Futema, Steve Humphries, Shane McCarthy, Hannah Mitchison, Francesco Muntoni, Alexandros Onoufriadis, Victoria Parker, Felicity Payne, Vincent Plagnol, Lucy Raymond, David Savage, Peter Scambler, Miriam Schmidts, Robert Semple, Eva Serra, Jim Stalker, Margriet van Kogelenberg, Parthiban Vijayarangakannan, Klaudia Walter, and Gretta Wood.

Acknowledgments

J.R., H.B., K.A.W., A.M., J.K.R., M.S.T., V.v.H., and D.R.F. are all supported by Medical Research Council (MRC) program grants awarded to the MRC Human Genetics Unit. Funding for UK10K was provided by the Wellcome Trust under award WT091310. Support for the Baylor-Hopkins Center for Mendelian Genomics was provided by the NIH National Human Genome Research Institute (U54 HG006542). G.H. is supported by HelseVest grant 911744. Thanks are given to Inge Jonassen and Kjell Petersen (Computational Biology Unit, Department of Informatics, University of Bergen, Norway) for providing IT infrastructure for the Norwegian next-generation sequencing data through the Elixir.no project and to the HudsonAlpha Institute for Biotechnology (Huntsville) for performing whole-exome sequencing in family 676.

Received: March 24, 2014
Accepted: May 13, 2014
Published: June 5, 2014

Web Resources

The URLs for data presented herein are as follows:

1000 Genomes, http://www.1000genomes.org/
European Genome-phenome Archive, https://www.ebi.ac.uk/ega/
FANTOM4, http://fantom.gsc.riken.jp/4/
NHLBI Exome Sequencing Project (ESP) Exome Variant Server, http://evs.gs.washington.edu/EVS/

Online Mendelian Inheritance in Man (OMIM), http://www.omim.org/
Picard, http://picard.sourceforge.net
RefSeq, http://www.ncbi.nlm.nih.gov/gene/
UCSC Genome Browser, http://genome.ucsc.edu/
UK10K project, http://www.uk10k.org/

References

1. Haddad, M.A., Sei, M., Sampaio, M.W., and Kara-José, N. (2007). Causes of visual impairment in children: a study of 3,210 cases. J. Pediatr. Ophthalmol. Strabismus *44*, 232–240.
2. Rudanko, S.L., and Laatikainen, L. (2004). Visual impairment in children born at full term from 1972 through 1989 in Finland. Ophthalmology *111*, 2307–2312.
3. Fantes, J., Ragge, N.K., Lynch, S.A., McGill, N.I., Collin, J.R., Howard-Peebles, P.N., Hayward, C., Vivian, A.J., Williamson, K., van Heyningen, V., and FitzPatrick, D.R. (2003). Mutations in SOX2 cause anophthalmia. Nat. Genet. *33*, 461–463.
4. Ragge, N.K., Lorenz, B., Schneider, A., Bushby, K., de Sanctis, L., de Sanctis, U., Salt, A., Collin, J.R., Vivian, A.J., Free, S.L., et al. (2005). SOX2 anophthalmia syndrome. Am. J. Med. Genet. A. *135*, 1–7, discussion 8.
5. Ragge, N.K., Brown, A.G., Poloschek, C.M., Lorenz, B., Henderson, R.A., Clarke, M.P., Russell-Eggitt, I., Fielder, A., Gerrelli, D., Martinez-Barbera, J.P., et al. (2005). Heterozygous mutations of OTX2 cause severe ocular malformations. Am. J. Hum. Genet. *76*, 1008–1022.
6. Glaser, T., Jepeal, L., Edwards, J.G., Young, S.R., Favor, J., and Maas, R.L. (1994). PAX6 gene dosage effect in a family with congenital cataracts, aniridia, anophthalmia and central nervous system defects. Nat. Genet. *7*, 463–471.
7. Pasutto, F., Sticht, H., Hammersen, G., Gillessen-Kaesbach, G., Fitzpatrick, D.R., Nürnberg, G., Brasch, F., Schirmer-Zimmermann, H., Tolmie, J.L., Chitayat, D., et al. (2007). Mutations in STRA6 cause a broad spectrum of malformations including anophthalmia, congenital heart defects, diaphragmatic hernia, alveolar capillary dysplasia, lung hypoplasia, and mental retardation. Am. J. Hum. Genet. *80*, 550–560.
8. Fares-Taie, L., Gerber, S., Chassaing, N., Clayton-Smith, J., Hanein, S., Silva, E., Serey, M., Serre, V., Gérard, X., Baumann, C., et al. (2013). ALDH1A3 mutations cause recessive anophthalmia and microphthalmia. Am. J. Hum. Genet. *92*, 265–270.
9. Srour, M., Chitayat, D., Caron, V., Chassaing, N., Bitoun, P., Patry, L., Cordier, M.P., Capo-Chichi, J.M., Francannet, C., Calvas, P., et al. (2013). Recessive and dominant mutations in retinoic acid receptor beta in cases with microphthalmia and diaphragmatic hernia. Am. J. Hum. Genet. *93*, 765–772.
10. Gerth-Kahlert, C., Williamson, K., Ansari, M., Rainger, J.K., Hingst, V., Zimmermann, T., Tech, S., Guthoff, R.F., van Heyningen, V., and Fitzpatrick, D.R. (2013). Clinical and mutation analysis of 51 probands with anophthalmia and/or severe microphthalmia from a single center. Mol. Genet. Genomic Med. *1*, 15–31.
11. Chassaing, N., Causse, A., Vigouroux, A., Delahaye, A., Alessandri, J.L., Boespflug-Tanguy, O., Boute-Benejean, O., Dollfus, H., Duban-Bedu, B., Gilbert-Dussardier, B., et al. (2013). Molecular findings and clinical data in a cohort of 150 patients with anophthalmia/microphthalmia. Clin. Genet. Published online September 10, 2013. http://dx.doi.org/10.1111/cge.12275.
12. Williamson, K.A., Rainger, J., Floyd, J.A., Ansari, M., Meynert, A., Aldridge, K.V., Rainger, J.K., Anderson, C.A., Moore, A.T., Hurles, M.E., et al.; UK10K Consortium (2014). Heterozygous loss-of-function mutations in YAP1 cause both isolated and syndromic optic fissure closure defects. Am. J. Hum. Genet. *94*, 295–302.
13. Olbrich, H., Schmidts, M., Werner, C., Onoufriadis, A., Loges, N.T., Raidt, J., Banki, N.F., Shoemark, A., Burgoyne, T., Al Turki, S., et al.; UK10K Consortium (2012). Recessive HYDIN mutations cause primary ciliary dyskinesia without randomization of left-right body asymmetry. Am. J. Hum. Genet. *91*, 672–684.
14. Haugarvoll, K., Johansson, S., Tzoulis, C., Haukanes, B.I., Bredrup, C., Neckelmann, G., Boman, H., Knappskog, P.M., and Bindoff, L.A. (2013). MRI characterisation of adult onset alpha-methylacyl-coA racemase deficiency diagnosed by exome sequencing. Orphanet J. Rare Dis. *8*, 1.
15. Bainbridge, M.N., Hu, H., Muzny, D.M., Musante, L., Lupski, J.R., Graham, B.H., Chen, W., Gripp, K.W., Jenny, K., Wienker, T.F., et al. (2013). De novo truncating mutations in ASXL3 are associated with a novel clinical phenotype with similarities to Bohring-Opitz syndrome. Genome Med. *5*, 11.
16. Chow, K.L., Hall, D.H., and Emmons, S.W. (1995). The mab-21 gene of Caenorhabditis elegans encodes a novel protein required for choice of alternate cell fates. Development *121*, 3615–3626.
17. Choy, S.W., Wong, Y.M., Ho, S.H., and Chow, K.L. (2007). C. elegans SIN-3 and its associated HDAC corepressor complex act as mediators of male sensory ray development. Biochem. Biophys. Res. Commun. *358*, 802–807.
18. Margolis, R.L., Stine, O.C., McInnis, M.G., Ranen, N.G., Rubinsztein, D.C., Leggo, J., Brando, L.V., Kidwai, A.S., Loev, S.J., Breschel, T.S., et al. (1996). cDNA cloning of a human homologue of the Caenorhabditis elegans cell fate-determining gene mab-21: expression, chromosomal localization and analysis of a highly polymorphic (CAG)n trinucleotide repeat. Hum. Mol. Genet. *5*, 607–616.
19. Mariani, M., Corradi, A., Baldessari, D., Malgaretti, N., Pozzoli, O., Fesce, R., Martinez, S., Boncinelli, E., and Consalez, G.G. (1998). Mab21, the mouse homolog of a C. elegans cell-fate specification gene, participates in cerebellar, midbrain and eye development. Mech. Dev. *79*, 131–135.
20. Kennedy, B.N., Stearns, G.W., Smyth, V.A., Ramamurthy, V., van Eeden, F., Ankoudinova, I., Raible, D., Hurley, J.B., and Brockerhoff, S.E. (2004). Zebrafish rx3 and mab21l2 are required during eye morphogenesis. Dev. Biol. *270*, 336–349.
21. Cederlund, M.L., Vendrell, V., Morrissey, M.E., Yin, J., Gaora, P.Ó., Smyth, V.A., Higgins, D.G., and Kennedy, B.N. (2011). mab21l2 transgenics reveal novel expression patterns of mab21l1 and mab21l2, and conserved promoter regulation without sequence conservation. Dev. Dyn. *240*, 745–754.
22. Yamada, R., Mizutani-Koseki, Y., Koseki, H., and Takahashi, N. (2004). Requirement for Mab21l2 during development of murine retina and ventral body wall. Dev. Biol. *274*, 295–307.
23. Wong, R.L., Chan, K.K., and Chow, K.L. (1999). Developmental expression of Mab21l2 during mouse embryogenesis. Mech. Dev. *87*, 185–188.
24. Kuchta, K., Knizewski, L., Wyrwicz, L.S., Rychlewski, L., and Ginalski, K. (2009). Comprehensive classification of nucleotidyltransferase fold proteins: identification of novel families and their representatives in human. Nucleic Acids Res. *37*, 7701–7714.

25. Xiao, T.S., and Fitzgerald, K.A. (2013). The cGAS-STING pathway for DNA sensing. Mol. Cell *51*, 135–139.
26. Hartmann, R., Justesen, J., Sarkar, S.N., Sen, G.C., and Yee, V.C. (2003). Crystal structure of the 2′-specific and double-stranded RNA-activated interferon-induced antiviral protein 2′-5′-oligoadenylate synthetase. Mol. Cell *12*, 1173–1185.
27. Meng, H., Deo, S., Xiong, S., Dzananovic, E., Donald, L.J., van Dijk, C.W., and McKenna, S.A. (2012). Regulation of the interferon-inducible 2′-5′-oligoadenylate synthetases by adenovirus VA(I) RNA. J. Mol. Biol. *422*, 635–649.
28. Hartmann, R., Norby, P.L., Martensen, P.M., Jorgensen, P., James, M.C., Jacobsen, C., Moestrup, S.K., Clemens, M.J., and Justesen, J. (1998). Activation of 2′-5′ oligoadenylate synthetase by single-stranded and double-stranded RNA aptamers. J. Biol. Chem. *273*, 3236–3246.
29. Schuurs-Hoeijmakers, J.H., Oh, E.C., Vissers, L.E., Swinkels, M.E., Gilissen, C., Willemsen, M.A., Holvoet, M., Steehouwer, M., Veltman, J.A., de Vries, B.B., et al. (2012). Recurrent de novo mutations in PACS1 cause defective cranial-neural-crest migration and define a recognizable intellectual-disability syndrome. Am. J. Hum. Genet. *91*, 1122–1127.
30. Bashir, T., and Pagano, M. (2003). Aberrant ubiquitin-mediated proteolysis of cell cycle regulatory proteins and oncogenesis. Adv. Cancer Res. *88*, 101–144.
31. Nakamura, T., Colbert, M., Krenz, M., Molkentin, J.D., Hahn, H.S., Dorn, G.W., 2nd, and Robbins, J. (2007). Mediating ERK 1/2 signaling rescues congenital heart defects in a mouse model of Noonan syndrome. J. Clin. Invest. *117*, 2123–2132.
32. Nakamura, T., Gulick, J., Pratt, R., and Robbins, J. (2009). Noonan syndrome is associated with enhanced pERK activity, the repression of which can prevent craniofacial malformations. Proc. Natl. Acad. Sci. USA *106*, 15436–15441.
33. Corson, L.B., Yamanaka, Y., Lai, K.M., and Rossant, J. (2003). Spatial and temporal patterns of ERK signaling during mouse embryogenesis. Development *130*, 4527–4537.
34. Krejci, P. (2014). The paradox of FGFR3 signaling in skeletal dysplasia: why chondrocytes growth arrest while other cells over proliferate. Mutat. Res. *759*, 40–48.
35. Harima, Y., and Kageyama, R. (2013). Oscillatory links of Fgf signaling and Hes7 in the segmentation clock. Curr. Opin. Genet. Dev. *23*, 484–490.
36. Schubbert, S., Bollag, G., Lyubynska, N., Nguyen, H., Kratz, C.P., Zenker, M., Niemeyer, C.M., Molven, A., and Shannon, K. (2007). Biochemical and functional characterization of germ line KRAS mutations. Mol. Cell. Biol. *27*, 7765–7770.
37. Le Goff, C., and Cormier-Daire, V. (2012). From tall to short: the role of TGFβ signaling in growth and its disorders. Am. J. Med. Genet. C. Semin. Med. Genet. *160C*, 145–153.

The American Journal of Human Genetics, Volume *94*

Supplemental Data

Monoallelic and Biallelic Mutations in *MAB21L2* Cause a Spectrum of Major Eye Malformations

Joe Rainger, Davut Pehlivan, Stefan Johansson, Hemant Bengani, Luis Sanchez-Pulido, Kathleen A. Williamson, Mehmet Ture, Heather Barker, Karen Rosendahl, Jürgen Spranger, Denise Horn, Alison Meynert, James A.B. Floyd, Trine Prescott, Carl A. Anderson, Jacqueline K. Rainger, Ender Karaca, Claudia Gonzaga-Jauregui, Shalini Jhangiani, Donna M. Muzny, Anne Seawright, Dinesh C. Soares, Mira Kharbanda, Victoria Murday, Andrew Finch, UK10K, Baylor-Hopkins Center for Mendelian Genomics, Richard A. Gibbs, Veronica van Heyningen, Martin S. Taylor, Tahsin Yakut, Per M. Knappskog, Matthew E. Hurles, Chris P. Ponting, James R. Lupski, Gunnar Houge, and David R. FitzPatrick

Supplemental Data

Figure S1 Alignment of MAB21L2 orthologs

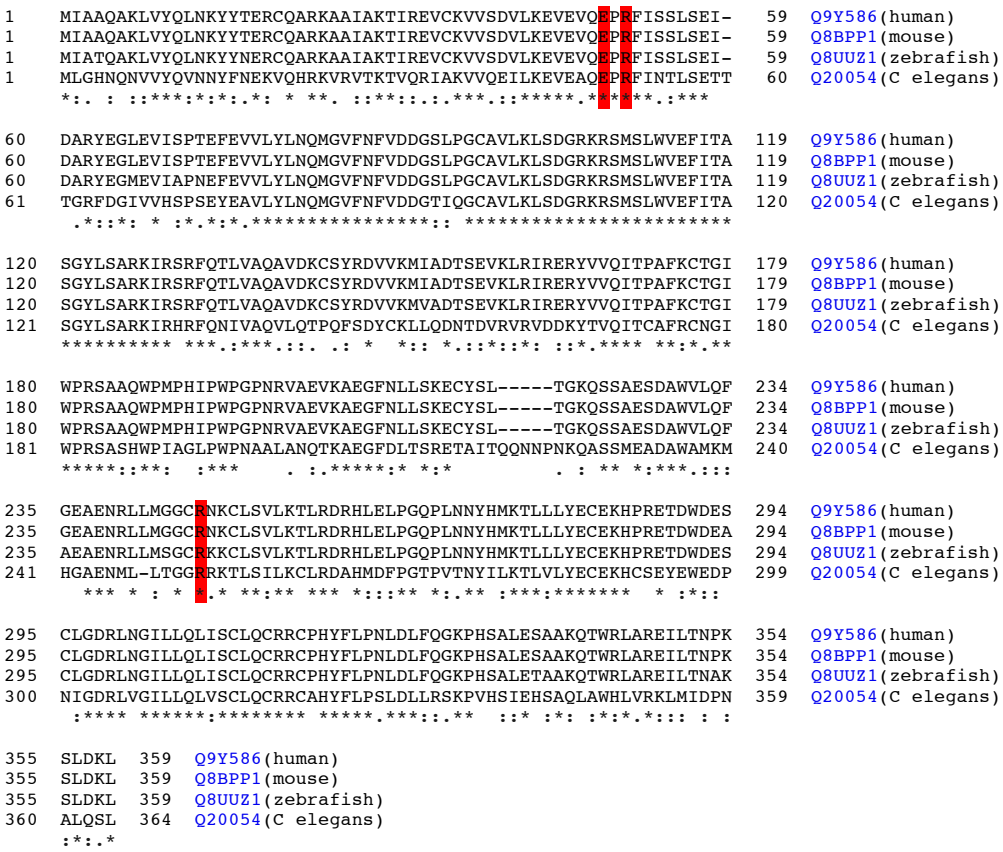

Figure S1 legend: Alignment of orthologous MAB21L2 proteins from human, mouse, zebrafish and C elegans showing cross species conservation of primary amino acid sequence. The residues in the sequences that are equivalent to those mutated in the human protein are indicated by the red highlight. The UniProt accession codes for each of the proteins is given to the right of the alignment. The alignment was performed on the UniProt web site using the default parameters.

Figure S2 MAB21L2 lacks Nucleotidyl Transferase activity

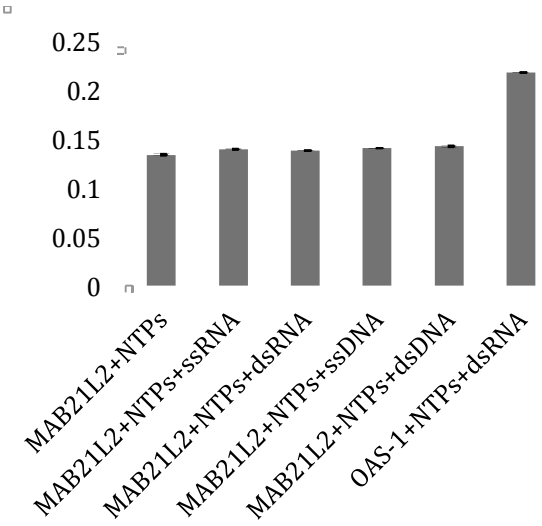

Figure S2 legend: A graph showing the absence of nuceotidyl transferase activity in MAB21L2 purified protein. OAS protein purified in the same way as MAB21L2 is a positive control and when incubated with an equal mixture of NTP (ATP, CTP, GTP, UTP) and double-stranded RNA (dsRNA) significant pyrophosphate release is detected indicating nucleotidyl transferase activity. MAB21L2 showed no activity above background with NTPs using dsRNA, dsDNA, single stranded RNA (ssRNA) or ssDNA as an activator. The error bars represent standard errors.

Figure S3

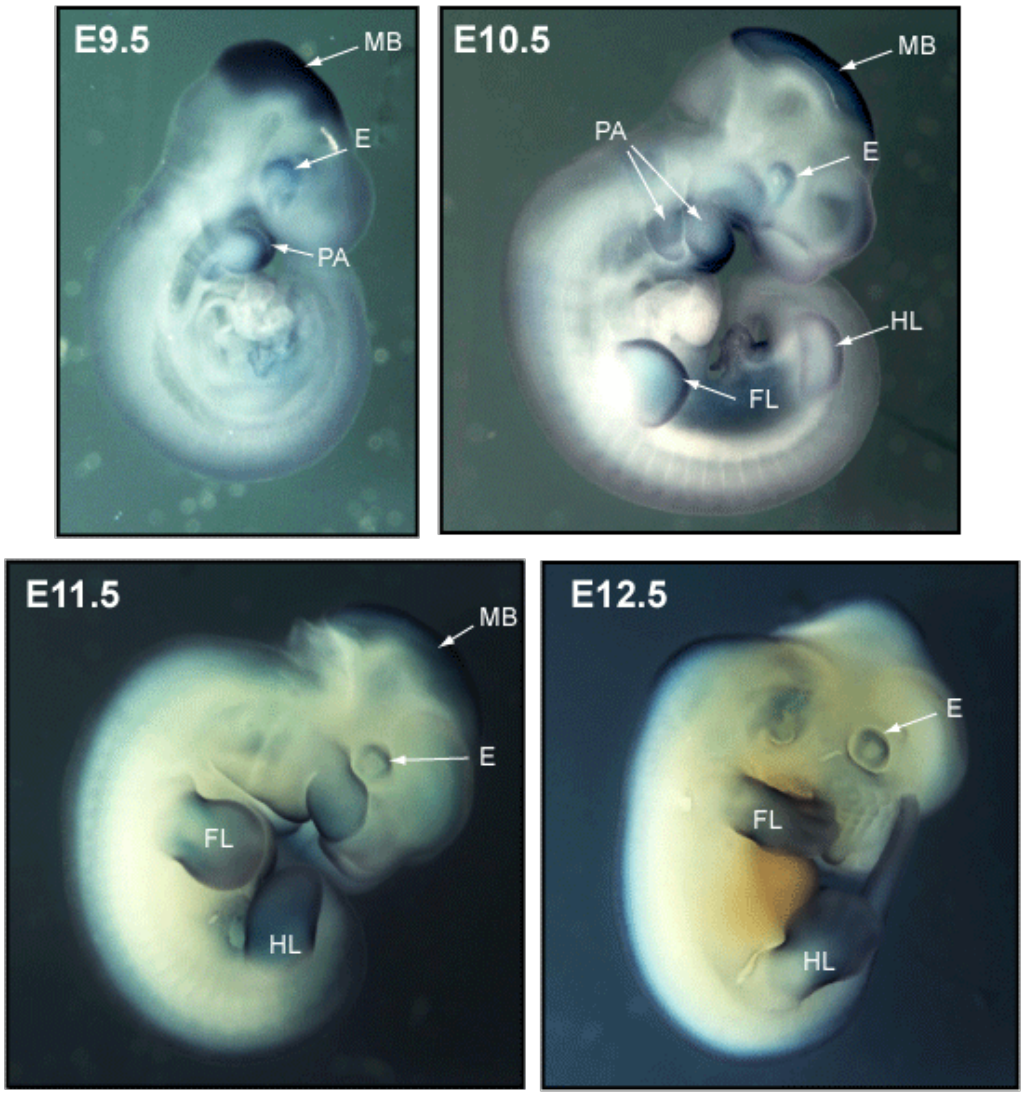

Figure S3. Developmental expression of *Mab21L2* in early mouse embryos at embryonic stage (E)9.5, E10.5, E11.5 and E12.5 by whole mount *in situ* hybridization showed specific expression domains at all stages. In particular, transcripts were identified in the developing eyes (E), forelimbs (FL), hindlimbs (HL), pharyngeal arches (PA) and midbrain (MB) regions. Midbrain expression was particularly strong at E9.5-E10.5.

Figure S4

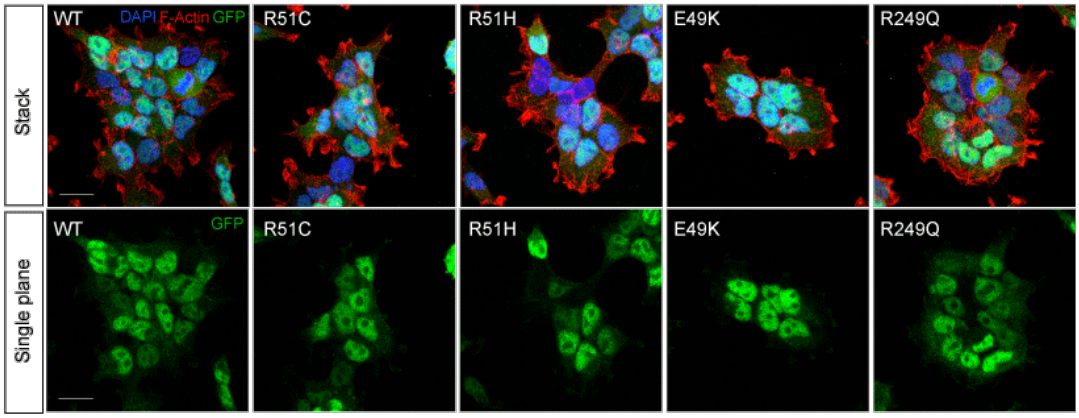

Figure S4: Immunofluorescence analyses with stacked (top) and single-plane (bottom) confocal microscopy images of MAB21L2-GFP stable cell lines indicated predominantly nuclear localization of WT and mutant MAB21L2-GFP (green) alleles with anti-GFP antibody (Clonetech Living Colours JL-8). Filamentous actin was stained red (Alexa Fluor 555-Phalloidin, Life Technologies) and DAPI (blue) was used to counterstained nuclei. Scale bar = 20 µm.

Table S1 Shared Heterozygous Variants in Family 1463 and Homozygous Variants in Family 4468

ID	Gene	genomic	mut	Genotype	Consequence	SIFT	PolyPhen
1463	ABCA6	chr17 g.67084341C>A	1222G>V	0/1	Missense	deleterious(0.01)	probably_damaging(0.998)
1463	ANKRD50	chr4 g.125592016C>A	806A>S	0/1	Missense	tolerated(0.89)	possibly_damaging(0.888)
1463	AURKB	chr17 g.8109861C>G	212G>R	0/1	Missense	deleterious(0.01)	probably_damaging(1)
1463	CCDC87	chr11 g.66359810T>C	226N>S	0/1	Missense	tolerated(0.25)	benign(0.002)
1463	CDH13	chr16 g.82892049A>C	90E>A	0/1	Missense	tolerated(0.19)	possibly_damaging(0.913)
1463	CHRNE	chr17 g.4805555G>C	101P>A	0/1	Missense	deleterious(0.01)	probably_damaging(0.998)
1463	CTU2	chr16 g.88781064C>T	424T>I	0/1	Missense	tolerated(0.19)	benign(0)
1463	FAM196B	chr5 g.169310185G>A	240R>C	0/1	Missense	tolerated(0.06)	benign(0)
1463	FRMPD1	chr9 g.37740753C>T	743T>I	0/1	Missense	tolerated(0.05)	benign(0.059)
1463	HMGB2	chr4 g.174253258CTCATCT>C	199-201EDE>E	0/1	In-frame deletion		
1463	IFT122	chr3 g.129207162CTTGG>C	690-691	0/1	Frameshift coding		
1463	IFT122	chr3 g.129207157GCTT>G	688-689AC>G	0/1	In-frame deletion		
1463	IFT122	chr3 g.129207169GTCACAGAC>G	692-694	0/1	Frameshift coding		
1463	IL12RB1	chr19 g.18174698G>T	536R>S	0/1	Missense	deleterious(0.05)	possibly_damaging(0.487)
1463	LIN9	chr1 g.226496911C>T	127R>H	0/1	Missense	deleterious(0.01)	unknown(0)
1463	MAB21L2	chr4 g.151504333G>A	51R>H	0/1	Missense	deleterious(0)	probably_damaging(1)
1463	METTL4	chr18 g.2544214G>A	418S>L	0/1	Missense	deleterious(0)	probably_damaging(1)
1463	MUC4	chr3 g.195512179G>A	2091	0/1	Possible Missense		
1463	MVD	chr16 g.88723943G>C	102L>V	0/1	Missense	tolerated(0.3)	benign(0)
1463	NEB	chr2 g.152522837C>T	1600V>I	0/1	Missense	tolerated(0.25)	probably_damaging(0.971)
1463	NLRC4	chr2 g.32476662G>T	91H>N	0/1	Missense	tolerated(0.35)	benign(0.073)
1463	PSMB5	chr14 g.23503876G>C	72	0/1	Possible Missense		
1463	PTCHD3	chr10 g.27703152G>T	10P>T	0/1	Missense		benign(0)
1463	SLC9A9	chr3 g.143551039C>G	67R>P	0/1	Missense	deleterious(0)	probably_damaging(0.999)
1463	SLCO2B1	chr11 g.74873700G>C	6G>A	0/1	Missense	deleterious(0)	probably_damaging(0.987)
1463	SPON1	chr11 g.14279384G>A	477V>I	0/1	Missense	tolerated(0.38)	possibly_damaging(0.619)
1463	TMEM116	chr12 g.112371748G>C	133H>Q	0/1	Missense	tolerated(0.43)	benign(0.174)
4468	LTB4R2	chr14 g.24780056GCA>G	N149fs	1/1	frameshift_deletion		
4468	MAB21L2	chr4 g.151504921	R247Q	1/1	Missense	deleterious(0.97)**	probably_damaging(1)
4468	NXF3	chrX g.102332646	V494L	1	Missense		neutral (0.24)
4468	TMPRSS9	chr19 g.2424094	G818fs	1/1	frameshift_insertion		

1/1 = homozygous; 1/0 = heterozygous; 1 = hemizygous; ** dbNSFP v1.3 annotates this variant with a SIFT Score (1-SIFT) of 0.97 and a prediction "Deleterious". dbNSFP v2.0 and dbNSFP v2.3 annotate this variant with a SIFT score of 0.14 (1-SIFT score = 0.86) and a "Tolerated" prediction. The current web version of SIFT (http://provean.jcvi.org/genome_submit.php) gives a SIFT score of 0.000 with a "Damaging" prediction and a PROVEAN score of -2.812 with a "Deleterious" prediction. Mutation taster and Polyphen2 predicted "disease causing" and "probably damaging", respectively.

Table S2: Clinical Features and Genotypes of Individuals with *MAB21L2* mutations

Family	131		1463		676		4480		4468			
Proband(s)	II.1		III.1		II.1		II.1		II.1		II.2	
chr4 genomic variant hg19	g.151504326G>A		g,151504333G>A		g,151504332C>T		g,151504332C>T		g.151504921G>A			
Mutation	c.145G>A p.(Glu49Lys)		c.152G>A p.(Arg51His)		c.151C>T p.(Arg51Cys)		c.151C>T p.(Arg51Cys)		c.[740G>A];[740G>A] p.[(Arg247Gln)];[(Arg247Gln)]			
Inheritance	unknown		paternal		de novo		de novo		maternal & paternal – parents have normal eyes			
Sex	Male		Male		Female		Male		Male		Male	
Genotype	heterozygous		heterozygous		heterozygous		heterozygous		homozygous		homozygous	
Birth Weight [z score]	NR		3033g @ 40 [-1.1]		3260g@38		3360 g		NR		3900g @ 40 [+0.88]	
Maternal/Paternal Age at birth	33/37		24/30		NR/NR		30/33		18/NR		20/NR	
Age at last assessment	39 y		13 y		10 y		24 y		5y		3y	
Height[z score]	NR		154.9cm [-0.29]		100cm[-6.7]		121 cm [-8.3]		112cm [-0.07]		97cm [+0.44]	
Weight[z score]	NR		63.5kg [+1.73]		NR		52 kg [-2.9]		17.5kg [-0.92]		13.8kg [-0.55]	
OFC[z score]	60 cm [+1.8]		NR		57 cm [+2.59 SD]		55 cm [-1.1]		51cm [-1.2]		48cm [-2.4]	
Eye	R	L	R	L	R	L	R	L	R	L	R	L
Anophthalmia	-	-	-	-	+	+	+	+	-	-	-	-
Microphthalmia	+	+	+	+	N/A	N/A	N/A	N/A	-	-	-	-
Coloboma	+	+	+	?	N/A	N/A	N/A	N/A	+	+	+	+
Microcornea	+	+	+	?	N/A	N/A	N/A	N/A	-	-	-	-
Sclerocornea	-	-	-	+	N/A	N/A	N/A	N/A	-	-	-	-
Vision	None	None	6/60	None	None	None	None	None	Yes	Yes	Yes	Yes
Skeletal												
Rhizomelia	No		No		Severe Bilateral		Arms & legs		None		None	
Joint contractures	No		Knees & Hips Bilaterally		All large joints		All large joints		None		None	
Hypoplastic femoral condyles	Unknown		Bilateral				Yes		None		None	
Details	Recurrent patella dislocations, 3/4 syndactyly of hands, 2/3 syndactyly of feet		Bowing of both legs noted as infant, calf wasting and pes planus		Short truck, normal sized hands and feet		Short humeri and femora,short tibiae, thin radius		None		Mild shortness of the long bones with decreased tubulation	
Other												
Hypospadias	No		+		N/A		No		No		No	
Undescended testes	Bilateral		No		N/A		No		No		No	
Precocious Puberty	No		No		7 years		No		No		No	
Intellectual disability	None		None		Moderate ID with autistic spectrum disorder		Moderate		None		None	
Other features									Strabismus on left, facial dysmorphism		Strabismus on right, facial dysmorphism	

NR = not recorded; N/A = not applicable; + = feature present; - = feature not present

Table S3: List of candidate genes used in UK10K exome analysis:

Inclusion criteria for this were; site- and stage-specific expression during early eye development in mouse embryos AND/OR the observation of a major eye malformation in any vertebrate animal model AND/OR mutation identification in humans with major eye malformations.

Gene symbol	Gene name	MIM number
ATOH1 (*MATH1*)	atonal homolog 1 (Drosophila)	601461
ATOH7 (*MATH5*)	atonal homolog 7 (Drosophila)	609875
BMP4	bone morphogenetic protein 4	112262
BMP7	bone morphogenetic protein 7	112267
FGF10	fibroblast growth factor 10	602115
FGF19 (*Fgf15*)	fibroblast growth factor 19	603891
HES1	hes family bHLH transcription factor 1	139605
HESX1	HESX homeobox 1	601802
LHX1	LIM homeobox 1	601999
MAB3: 21L1	mab-21-like 1 (C. elegans)	601280
MAB21L2	mab-21-like 2 (C. elegans)	604357
MAF1	MAF1 homolog (S. cerevisiae)	610210
mbx1	MADS-box transcription factor Mbx1	N/A (*S. pombe*)
NEUROG2 (*NGN2*)	neurogenin 2	606624
OTX1	orthodenticle homeobox 1	600036
OTX2	orthodenticle homeobox 2	600037
PAX2	paired box 2	167409
PAX6	paired box 6	607108
POU4F1	POU class 4 homeobox 1	601632
POU4F2	POU class 4 homeobox 2	113725
RAX	retina and anterior neural fold homeobox	601881
RXR: RXRA; *RXRB*; *RXRG*	retinoid X receptor, alpha; retinoid X receptor, beta; retinoid X receptor, gamma	180245; 180246; 180247
SOX1	SRY (sex determining region Y)-box 1	602148
SOX2	SRY (sex determining region Y)-box 2	184429
SOX3	SRY (sex determining region Y)-box 3	313430
SOX14	SRY (sex determining region Y)-box 14	604747
SOX21	SRY (sex determining region Y)-box 21	604974
SHH	sonic hedgehog	600725
SIX3	SIX homeobox 3	603714
SIX6	SIX homeobox 6	606326
STRA6	stimulated by retinoic acid 6	610745
TBX2	T-box 2	600747
TBX3	T-box 3	601621
TBX5	T-box 5	601620
VAX1	ventral anterior homeobox 1	604294
VAX2	ventral anterior homeobox 2	604295
VSX1	visual system homeobox 1	605020
VSX2 (*CHX10*)	visual system homeobox 2	142993

Table S4 Coverage and Depth of Exome Sequencing

Family	Median Depth	Coverage at >8X
4468	97-112x	90-93%
676	49-102X	>94%
1463	110-112X	>90%